


 Cite this: *RSC Adv.*, 2026, 16, 15736

# Construction of a Cu/Fe/S multi-active-site synergistic Fenton-like system *via* mechanically activated natural copper sulfide ore for efficient tetracycline degradation

 Lizheng Gou,<sup>abc</sup> Xiwang Miao,<sup>c</sup> Yuhang Liu,<sup>ab</sup> Mei Zhang<sup>ab</sup> and Min Guo<sup>\*ab</sup>

Addressing the underexplored catalytic potential of natural polymetallic sulfide minerals and the unclear structure–activity relationship between symbiotic structures and catalytic performance, this study explores the use of mechanically activated natural copper sulfide ore to construct a bimetallic synergistic Fenton-like system for tetracycline degradation, with a focus on the synergistic role of Cu/Fe/S multi-active sites. By optimizing ball milling parameters (ball-to-powder ratio of 3:1, duration of 24 h), the catalyst achieved a remarkable 90.11% tetracycline degradation within 10 minutes. Mechanistic investigations revealed that mechanical activation refined particle size, increased specific surface area, and exposed more Cu/Fe/S active sites, establishing a “homogeneous (66.36%) – heterogeneous (33.64%)” synergistic catalytic mechanism. In the homogeneous phase, dissolved Cu<sup>2+</sup>/Fe<sup>2+</sup> accelerated H<sub>2</sub>O<sub>2</sub> decomposition. In the heterogeneous phase, the Cu<sup>+</sup>/Fe<sup>3+</sup> redox couple (0.16 V/0.77 V) created an energy level difference. Coupled with reductive sulfur species (S<sup>2-</sup>, S<sub>2</sub><sup>2-</sup>)-mediated electron transfer, this facilitated the Fe<sup>3+</sup> → Fe<sup>2+</sup> and Cu<sup>2+</sup> → Cu<sup>+</sup> cycles, thereby enhancing radical generation efficiency. Two distinct degradation pathways for tetracycline by the copper sulfide concentrate were identified, with intermediates undergoing deep oxidation and ring-opening reactions to mineralize into H<sub>2</sub>O, CO<sub>2</sub>, and NO<sub>3</sub><sup>-</sup>. This study overcomes the limitations of traditional single iron-based sulfide catalysts, revealing the catalytic enhancement mechanism of natural mineral symbiotic structures under mechanical activation. It offers a cost-effective and efficient heterogeneous Fenton-like solution for antibiotic wastewater treatment.

Received 23rd December 2025

Accepted 16th March 2026

DOI: 10.1039/d5ra09931e

[rsc.li/rsc-advances](https://rsc.li/rsc-advances)

## 1. Introduction

Tetracycline antibiotics are widely used in medicine, animal husbandry, and aquaculture due to their low cost and broad antibacterial spectrum.<sup>1</sup> However, large amounts of these antibiotics are discharged into the environment in their original or metabolized forms, leading to persistent residues in water bodies. These residues disrupt aquatic ecosystems (*e.g.*, inhibiting aquatic organism growth and altering microbial communities) and threaten human health *via* food chain accumulation and increased antibiotic resistance. Effective treatment of tetracycline pollution has become an urgent challenge in environmental remediation.<sup>2</sup>

Heterogeneous Fenton-like catalytic oxidation is a highly promising advanced oxidation technology. It works by

activating hydrogen peroxide (H<sub>2</sub>O<sub>2</sub>) at solid catalyst surface sites to generate hydroxyl radicals (<sup>•</sup>OH, oxidation potential 2.8 V) and other reactive oxygen species.<sup>3,4</sup> These species rapidly and non-selectively oxidize organic pollutants into CO<sub>2</sub> and H<sub>2</sub>O without causing secondary pollution.<sup>5,6</sup> Compared with traditional homogeneous Fenton reactions, heterogeneous Fenton processes reduce iron sludge generation and allow operation over a wider pH range.<sup>7,8</sup> Therefore, they are increasingly applied to tetracycline-containing wastewater treatment.<sup>9,10</sup>

In heterogeneous Fenton systems, the structure–activity relationship of the catalyst is crucial. Iron-based sulfides, due to their semiconducting and redox properties, have attracted much attention. Pyrite (FeS<sub>2</sub>), a typical low-valence iron sulfide,<sup>11</sup> has been widely used for heavy metal and nitrate<sup>12</sup> reduction, and can catalytically decompose H<sub>2</sub>O<sub>2</sub> to produce <sup>•</sup>OH for organic degradation.<sup>13,14</sup> Liu *et al.*<sup>15</sup> demonstrated that hydrothermally synthesized FeS<sub>2</sub> efficiently catalyzed H<sub>2</sub>O<sub>2</sub> to degrade metolachlor, with an <sup>•</sup>OH production rate 71 times higher than that of natural FeS<sub>2</sub>, mainly due to enhanced Fe<sup>2+</sup>/Fe<sup>3+</sup> cycling facilitated by molecular oxygen activation. Matta *et al.*<sup>16</sup> found that pyrite efficiently degraded 2,4,6-

<sup>a</sup>State Key Laboratory of Advanced Metallurgy, School of Metallurgical and Ecological Engineering, University of Science and Technology Beijing, Beijing 100083, P. R. China. E-mail: guomin@ustb.edu.cn

<sup>b</sup>School of Metallurgical and Ecological Engineering, University of Science and Technology Beijing, Beijing 100083, China

<sup>c</sup>MCC CISDI Group Co., Ltd, Chongqing 400013, P. R. China



trinitrotoluene *via* H<sub>2</sub>O<sub>2</sub> activation. Compared with hematite and goethite, pyrite-based Fenton systems exhibited faster ·OH-based degradation, attributed to iron oxidation states and Fe<sup>2+</sup> solubility. Che *et al.*<sup>17</sup> reported that pyrite outperformed homogeneous Fe<sup>2+</sup>/H<sub>2</sub>O<sub>2</sub> in degrading trichloroethylene and carbon tetrachloride. Additionally, pyrite oxidation released Fe and H<sup>+</sup> ions, maintaining an acidic pH favorable for Fenton reactions. Another important catalyst, chalcopyrite (CuFeS<sub>2</sub>), benefits from bimetallic Cu–Fe synergy.<sup>8,18–20</sup> The redox potential difference between Cu<sup>+</sup>/Cu<sup>2+</sup> (0.16 V) and Fe<sup>2+</sup>/Fe<sup>3+</sup> (0.77 V) facilitates electron transfer from Fe<sup>3+</sup> to Fe<sup>2+</sup>, accelerating H<sub>2</sub>O<sub>2</sub> decomposition and enhancing catalytic performance. Nie *et al.*<sup>21</sup> synthesized CuFeS<sub>2</sub> nanoparticles hydrothermally for effective bisphenol A degradation, attributing this to abundant surface Cu<sup>+</sup> and Fe<sup>2+</sup> sites, with sulfur facilitating redox cycling. Wang *et al.*<sup>22</sup> found that NaBH<sub>4</sub>-treated CuFeS<sub>2</sub> with sulfur vacancies could activate peroxymonosulfate (PMS) into non-radical singlet oxygen (<sup>1</sup>O<sub>2</sub>), enhancing resistance to complex wastewater interference. However, current studies focus mainly on synthetic or single-component iron sulfides, with limited exploration of natural polymetallic sulfide ores like copper sulfide, and little understanding of their coexistence structure–activity relationship.

Copper sulfide ore, a typical polymetallic sulfide, is composed of pyrite (FeS<sub>2</sub>) and chalcopyrite (CuFeS<sub>2</sub>). In its mineral structure, Fe exists as both Fe<sup>2+</sup> (60–70%) and Fe<sup>3+</sup> (30–40%), while Cu is predominantly Cu<sup>+</sup> (~90%) embedded in the Fe–S lattice. This unique valence distribution offers dual advantages: pyrite provides Fe<sup>2+</sup> for Fenton-like ·OH generation, while chalcopyrite's Cu<sup>+</sup> acts as an electron mediator to accelerate Fe<sup>3+</sup> to Fe<sup>2+</sup> reduction. Compared with single-phase pyrite or chalcopyrite, this coexisting structure may form “electron transport channels” to enhance interfacial charge separation and intrinsic catalytic activity. However, natural copper sulfide ore is typically dense, with encapsulated active sites and large particle size, leading to low solid–liquid mass transfer efficiency and limited catalytic performance.

Ball milling is an efficient physical activation method. Through high-frequency impact and shear, it modifies copper sulfide ore in multiple ways: (1) reducing particle size to submicron or nanoscale, increasing surface area and exposing active sites; (2) restructuring the crystal lattice to introduce sulfur vacancies and iron defects, enhancing adsorption; and (3) altering surface functional groups, forming hydroxyl or sulfoxo groups to optimize interfacial catalysis. However, the impact of milling parameters (time, ball-to-powder ratio) on catalyst structure–activity relationship remains unclear. Moreover, the electronic transfer mechanisms and radical generation pathways under different activation levels also require deeper understanding.

Therefore, this study investigates the effect and mechanism of mechanochemical activation on tetracycline degradation using copper sulfide ores. By optimizing ball milling conditions, catalytic activity was enhanced. The effects of catalyst dose, H<sub>2</sub>O<sub>2</sub> concentration, and pH on tetracycline removal were examined. Structural changes pre- and post-activation were characterized *via* XRD, XPS, SEM, *etc.* Free radical trapping and

LC-MS were used to identify reactive species (*e.g.*, ·OH) and degradation intermediates. Catalyst recyclability was also evaluated. Compared with previous studies on synthetic or single-phase sulfides, this work uniquely investigates: (i) the mechanochemical activation of natural polymetallic ore; (ii) the quantitative contribution of homogeneous *vs.* heterogeneous pathways; (iii) the role of sulfur species as electron mediators in a naturally occurring symbiotic structure. These aspects provide new insights into the design of cost-effective and efficient Fenton-like catalysts derived from natural minerals.

## 2. Experimental

### 2.1. Materials and reagents

The copper sulfide ore used in this study was provided by a local mineral processing company. It is a composite ore composed mainly of pyrite (FeS<sub>2</sub>) and chalcopyrite (CuFeS<sub>2</sub>). As shown in Table 1, the main chemical components are Fe (32.65 wt%), Cu (21.57 wt%), and S (28.34 wt%). Other reagents used include tetracycline, hydrogen peroxide, deionized water, isopropanol, L-histidine, and 4-hydroxy-TEMPO, all of analytical grade.

### 2.2. Ball milling experiments

Ball milling experiments were conducted using a Retsch PM 400 planetary ball mill equipped with ZrO<sub>2</sub> jars and ZrO<sub>2</sub> grinding balls. Milling was performed at a rotation speed of 300 rpm under ambient atmosphere. To prevent overheating and particle agglomeration during the process, 5 mL of ethanol was added as a process control agent.

Two series of experiments were carried out under varied milling conditions. (1) Variation of milling time: 20 g of ore, 40 g of milling balls, and 5 mL of ethanol were milled for durations of 12 h, 24 h, and 36 h. (2) Variation of ball-to-powder ratio: 20 g of ore was milled for 24 h with 5 mL of ethanol, using 20 g, 40 g, and 60 g of milling balls. In all experiments, the milling ball size distribution was maintained at a fixed ratio of 2 : 1 between 5–6 mm and 6–7 mm balls. After milling, the resulting samples were dried and stored in sealed glass containers for further analysis.

### 2.3. Catalytic degradation experiments

In each catalytic test, a certain amount of catalyst was added to a 300 mL beaker containing 200 mL tetracycline solution (20 mg L<sup>−1</sup>). The solution was stirred at 500 rpm in the dark for 30 min to establish adsorption–desorption equilibrium. Then, a set concentration of H<sub>2</sub>O<sub>2</sub> was added to initiate the catalytic reaction. All reactions were conducted at room temperature without pH adjustment. Samples (3 mL) were taken every 2 min, immediately quenched with 0.1 mL methanol, and transferred to 10 mL centrifuge tubes, centrifuged at 6000 rpm for 3 min,

Table 1 Chemical compositions of the copper sulfide ore (wt%)

Fe	Cu	S	O	Si	Zn	Ca	Mg	Al
32.6	21.6	28.3	10.1	2.5	1.6	1.7	1.1	0.5



and filtered through 0.45  $\mu\text{m}$  membranes. The absorbance of the filtrate was measured at 357 nm using a UV-vis spectrophotometer. The tetracycline degradation rate ( $\eta$ ) was calculated using eqn (1). All degradation experiments were performed in triplicate under identical conditions. Error bars in figures represent the standard deviation of three independent measurements.

$$\eta = (1 - C_t/C_0) \times 100\% \quad (1)$$

The degradation process of the antibiotic solution was fitted according to the pseudo-first-order kinetic model, as shown in eqn (2). And the removal efficiency of total organic carbon (TOC) in tetracycline solution was calculated using eqn (3).

$$\ln(C_t/C_0) = -k_{\text{app}} \times t \quad (2)$$

$$\text{TOC removal efficiency} = (\text{TOC}_0 - \text{TOC}_t)/\text{TOC}_0 \quad (3)$$

where  $k_{\text{app}}$  is the apparent rate constant ( $\text{min}^{-1}$ ),  $\text{TOC}_0$  represents the initial TOC content in tetracycline solution ( $\text{mg L}^{-1}$ ), and  $\text{TOC}_t$  denotes the TOC content at reaction time  $t$  ( $\text{mg L}^{-1}$ ).

#### 2.4. Quantitative analysis of $\cdot\text{OH}$ generated in heterogeneous Fenton-like reaction systems

The generation of  $\cdot\text{OH}$  in the catalytic reaction system was analyzed using fluorescence spectrophotometry with terephthalic acid as the trapping agent. First, standard solutions of dihydroxyterephthalic acid at various concentrations (0–200.0  $\mu\text{M}$ ) were prepared using a purified reagent. The fluorescence intensity of these standard solutions was then measured at 425 nm using a fluorescence spectrophotometer. A calibration curve was plotted to establish the relationship between fluorescence intensity and the concentration of dihydroxyterephthalic acid. Based on this curve, the concentration of  $\cdot\text{OH}$  produced in the catalytic system was determined. Control experiments with filtered reaction solutions confirmed that solid scattering did not significantly affect fluorescence measurements.

#### 2.5. Characterization and analysis method

An X-ray fluorescence spectrometer (XRF, Zetium, Netherlands) was used to analyze the chemical composition of the ore. An X-ray powder diffractometer (XRD, TTR3, Japan) and a scanning electron microscope (SEM, SUPRA55, Germany) were used to analyze the crystal phase, surface morphology, and elemental distribution, respectively. The elemental valence states were determined by an X-ray photoelectron spectrometer (XPS, AXIS ULTRA-DLD, Japan). The specific surface area and pore size distribution were analyzed using the nitrogen adsorption method (specific surface area and pore size analyzer, Autosorb-iQ, USA). A laser particle size analyzer (Topsizer, UK) was used to analyze the particle size of the samples. An ultraviolet-visible spectrophotometer (TU-1901, China) was used to measure the absorbance of the solution. The ion concentration and organic matter content in the solution were measured by an inductively coupled plasma mass spectrometer (ICP, iCAP-RQ, China) and

a total organic carbon analyzer (TOC, TOC-VCPH, Japan), respectively. The active free radicals in the catalytic system were measured by an electron spin resonance spectrometer (ESR, Bruker-A300, Germany; detailed parameters in Section S1). A liquid chromatography-mass spectrometry (LC-MS, USA) was used to analyze the intermediate products during the degradation process of tetracycline.

## 3. Results and discussion

### 3.1. Characterization of copper sulfide ore

To determine the forms of Fe and Cu in the ore, XRD analysis was conducted. As shown in Fig. 1, the ore mainly contains two crystalline phases including  $\text{FeS}_2$  (JCPDF: 71-2219) and  $\text{CuFeS}_2$  (JCPDF: 71-050), corresponding to its primary elements (Fe, Cu, S).  $\text{CuFeS}_2$  is the dominant phase. Other oxides present in minor amounts were not detected due to their low concentrations.

In addition, the ore consists of particles ranging from several to tens of microns in size as illustrated in Fig. 2. Elements S, Fe, and Cu overlap significantly, indicating wide distribution. Elements like Si, Mg, and O were found mainly in oxide form in small amounts (*e.g.*, test point #3). EDS confirmed that regions #1, #2, and #4 were mainly  $\text{FeS}_2$  or  $\text{CuFeS}_2$ , suggesting relatively independent phase distribution, which facilitates effective dispersion during catalysis.

Fig. 3 shows the full XPS spectrum and high-resolution scans. Through the analysis of element occurrence states and surface chemistry, it provides a basis for clarifying its heterogeneous catalytic active sites and redox characteristics. Copper sulfide ore is mainly composed of Cu, Fe, and S elements (Fig. 3a), and this result is consistent with the XRD detection result (Fig. 1). Fig. 3b presents Fe 2p spectrum, which exhibits three groups of characteristic peaks at 707.2 eV ( $\text{Fe}^{2+}$ , 19.24%), 711.5 eV/712.8 eV ( $\text{Fe}^{3+}$ , 80.76%). This mixed valence state distribution indicates that the material has intrinsic redox activity, and the  $\text{Fe}^{3+}/\text{Fe}^{2+}$  redox couple ( $E^\theta(\text{Fe}^{3+}/\text{Fe}^{2+}) = +0.77 \text{ V/SHE}$ ) can participate in the catalytic reaction as an electron transfer medium. Cu 2p spectrum exhibits obvious splitting at 931.9 eV ( $\text{Cu}^+$ , 66.42%) and 933.1 eV ( $\text{Cu}^{2+}$ , 33.58%) (Fig. 3c). Combined with the XRD phase analysis, it is confirmed that Cu

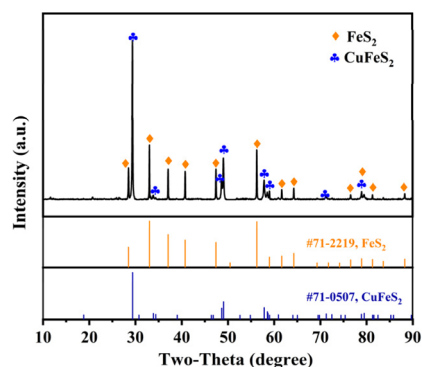


Fig. 1 XRD pattern of copper sulfide ore.



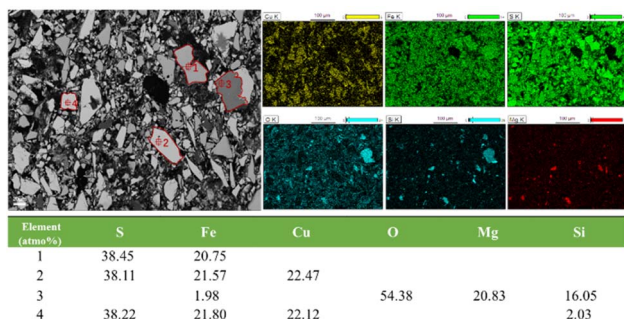


Fig. 2 SEM image, element distribution, and EDS results of copper sulfide ore.

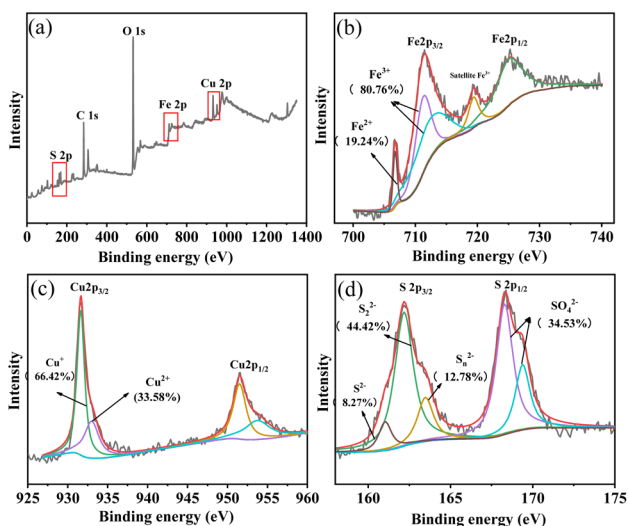


Fig. 3 XPS spectra of copper sulfide ore: (a) full spectrum, magnified spectra of (b) Fe 2p, (c) Cu 2p, and (d) S 2p.

exists stably in the +1 valence state in the  $\text{CuFeS}_2$  lattice. This low-valence copper ( $E^\theta$  ( $\text{Cu}^{2+}/\text{Cu}^+$ ) = +0.16 V/SHE) forms a synergistic oxidation system with high-valence iron, which is beneficial to the electron transfer process. As for S 2p spectrum (Fig. 3d), the characteristic peaks at 161.1 eV, 162.2 eV, and 163.9 eV correspond to surface-state monosulfides ( $\text{S}^{2-}$ , 8.27%), the S species bound to metals in the bulk phase (including Cu/Fe-S in the  $\text{CuFeS}_2$  structure and disulfides  $\text{S}_2^{2-}$  in the  $\text{FeS}_2$  structure, 44.42%), and polysulfides formed by sulfur vacancies on the  $\text{CuFeS}_2/\text{FeS}_2$  surface ( $\text{S}_n^{2-}$ , 12.78%), respectively. The characteristic peaks at 168.8 eV/169.9 eV correspond to sulfates formed by the oxidation of S elements in the minerals in the air ( $\text{SO}_4^{2-}$ , 34.53%). Among them, sulfur vacancies, as active sites, can enhance the adsorption of reactants and are expected to improve the catalytic reaction activity.

### 3.2. Influence of ball milling parameters on catalyst microstructure and catalytic performance

Ball milling, as a typical mechanochemical activation method, induces structural reorganization and surface modification of catalysts through high-energy shear and compressive forces.

Catalysts experience varying degrees of activation under different milling conditions, resulting in different catalytic efficiencies. To determine optimal ball milling parameters, the catalytic performance under varying milling times and ball-to-powder ratios was evaluated and analyzed from the perspectives of specific surface area, particle size, and surface chemical state.

**3.2.1. Effect of ball milling time.** Fig. 4a and b present the tetracycline degradation curves and corresponding kinetic fits for catalysts milled for different durations. As milling time increased from 0 h to 24 h, the degradation rate within 10 min improved from 51.35% to 90.11%, and the rate constant rose from  $0.036 \text{ min}^{-1}$  to  $0.176 \text{ min}^{-1}$ . Further extension to 36 h showed no significant improvement, indicating 24 h is optimal.

Fig. 4c shows  $\text{N}_2$  adsorption–desorption isotherms for catalysts milled under different times. All samples exhibited type IV isotherms with H3 hysteresis loops, suggesting mesoporous structures. The BET surface area in Fig. 4d increased from  $1.85 \text{ m}^2 \text{ g}^{-1}$  (0 h) to  $15.15 \text{ m}^2 \text{ g}^{-1}$  (24 h), and particle size decreased from  $8.56 \mu\text{m}$  to  $1.99 \mu\text{m}$ . Correspondingly, the degradation rate of tetracycline by the catalyst increased from 51.35% to 90.11%. From the above analysis, it can be seen that both the particle size and specific surface area of the catalyst can affect the catalytic efficiency. Appropriately increasing the ball-milling time will reduce the particle size and increase the specific surface area, resulting in an increase in the dispersion degree of the catalyst and an increase in the number of active sites, thus leading to an improvement in catalytic performance. When the optimal ball milling time of 24 h is reached, the particle size of the catalyst is  $1.99 \mu\text{m}$ , and the specific surface area is  $15.15 \text{ m}^2 \text{ g}^{-1}$ .

The ball milling process can cause changes in the crystal structure and surface physicochemical properties of the catalyst, thus affecting its catalytic performance. According to relevant literature reports,<sup>23,24</sup> during the degradation process of the catalyst in this system, the changes in the relative contents of surface-state  $\text{Cu}^+$ , surface-state  $\text{Fe}^{2+}$  and  $\text{Fe}^{3+}$  and the morphological changes of S play an important role in the catalytic effect. Therefore, the changes in the elemental forms on the catalyst surface were analyzed, and the results are shown in Fig. 5, and the detailed XPS fitting parameters are provided in Section S2.

For Cu 2p spectra (Fig. 5a and d), the peaks at 931.6 eV (surface  $\text{Cu}^+$ ), 932.1 eV (bulk  $\text{Cu}^+$ ), and 934.4 eV ( $\text{Cu}^{2+}$ ).<sup>25–27</sup> With increased milling time, surface  $\text{Cu}^+$  rose from 16.91% to 31.87%, while bulk  $\text{Cu}^+$  dropped from 58.54% to 39.12%, indicating that Cu–S bond breakage during milling exposed more surface  $\text{Cu}^+$  with high catalytic activity. As for Fe 2p spectra (Fig. 5b and d), bulk  $\text{Fe}^{2+}$  and  $\text{Fe}^{3+}$  peaks appeared at 706.9/712.1 eV. Surface  $\text{Fe}^{2+}$  and  $\text{Fe}^{3+}$  peaks appeared at 707.6/710.1 eV and 708.6/710.5/711.2 eV respectively.<sup>28,29</sup> From 12 h to 24 h milling, surface  $\text{Fe}^{2+}$  and  $\text{Fe}^{3+}$  increased by 3.69% and 5.86%, while bulk  $\text{Fe}^{2+}$  and  $\text{Fe}^{3+}$  decreased by 8.64% and 6.70%. These surface states are more catalytically active, and surface  $\text{Cu}^+$  enhances  $\text{Fe}^{2+}/\text{Fe}^{3+}$  cycling, thereby improving the degradation rate of the catalyst.

For S 2p spectra (Fig. 5c and d), the peaks at 161.1 eV (surface  $\text{S}^{2-}$ ), 162.4 eV (bulk metal-S, including Cu/Fe–S bonds of  $\text{CuFeS}_2$



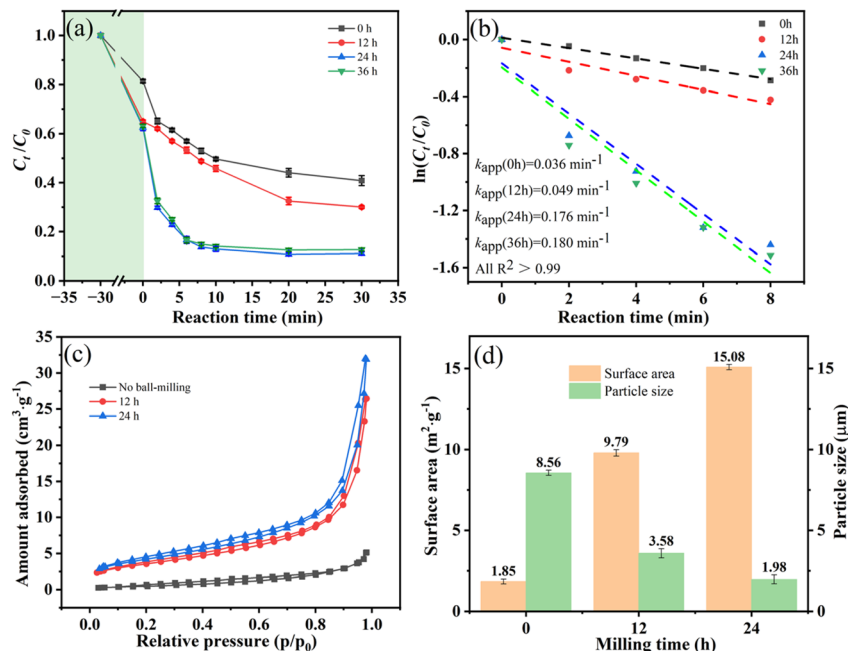


Fig. 4 Under different ball milling time conditions: (a) tetracycline degradation curves, (b) catalytic reaction kinetics curves, (c) catalyst  $N_2$  adsorption-desorption curves, (d) catalyst specific surface area and average particle size. (Ball-to-powder ratio: 3:1. Catalytic conditions: tetracycline concentration of  $20 \text{ mg L}^{-1}$ , catalyst dosage of  $0.50 \text{ g L}^{-1}$ ,  $H_2O_2$  dosage of  $3 \text{ mM}$ , initial pH value of 6.17; error bars represent standard deviation ( $n = 3$ )).

and disulfide  $S_2^{2-}$  of  $FeS_2$ ), 163.6 eV (polysulfides  $S_n^{2-}$ , formed by sulfur vacancies on the surface of  $CuFeS_2/FeS_2$ ), and 168.5/169.6 eV (sulfate  $SO_4^{2-}$ ).<sup>30</sup> From 12 h to 24 h milling, bulk metal-

S content decreased from 63.87% to 50.12%, surface  $S^{2-}$  increased from 13.83% to 17.74%, and  $SO_4^{2-}$  increased from 47.83% to 49.29%. According to relevant literature,<sup>31</sup> sulfur

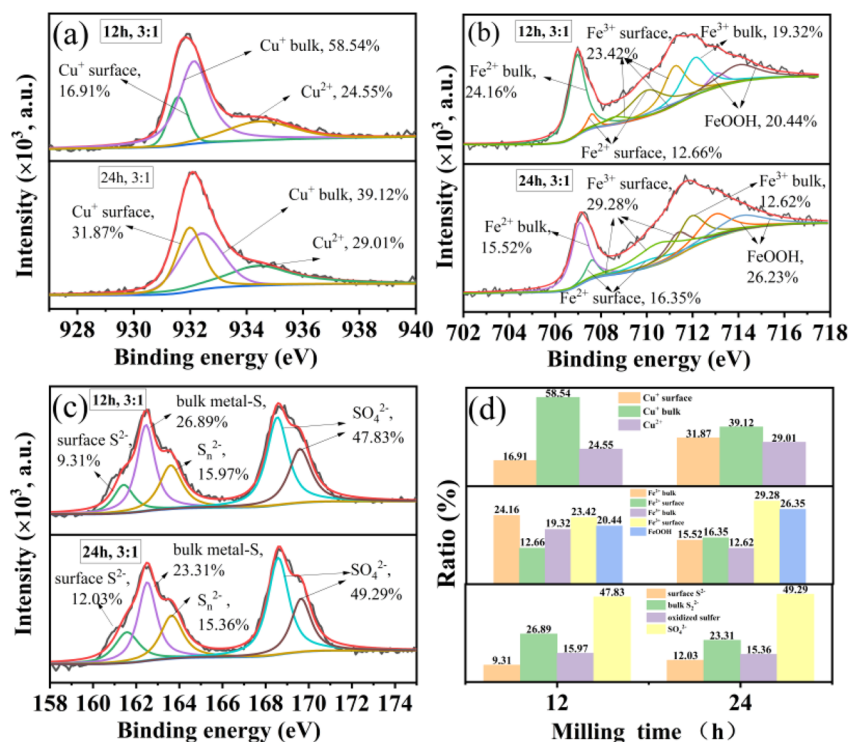


Fig. 5 XPS spectra of catalysts obtained under different ball milling time conditions: (a) Cu, (b) Fe, (c) S, (d) bar chart of the proportion of different morphological elements.



itself does not participate in the degradation reaction, but the copper-containing sulfate generated during the oxidation process will dissolve in the degradation solution, increasing the proportion of the homogeneous Fenton reaction and improving the degradation rate of tetracycline. At the same time, the above also verifies that increasing the ball milling time increases surface  $\text{Fe}^{2+}/\text{Fe}^{3+}$ , thereby improving the degradation rate of the catalyst.

**3.2.2. Effect of ball-to-powder ratio.** Fig. 6a and b present the degradation and kinetic curves for catalysts prepared with different ball-to-powder ratios. Increasing the ratio from 1 : 1 to 2 : 1 raised the 10 min degradation rate from 62.25% to 90.68% and the rate constant from  $0.066 \text{ min}^{-1}$  to  $0.182 \text{ min}^{-1}$ . Further increasing to 3 : 1 showed negligible improvement, thus 3 : 1 was chosen as optimal.

Fig. 6c displays  $\text{N}_2$  adsorption-desorption isotherms, again confirming mesoporosity structure. Fig. 6d shows BET surface areas and particle sizes. Compared to the raw ore, surface area increased by 66.05% and 87.78%, and particle size decreased by 53.62% and 76.75% at ratios of 1 : 1 and 3 : 1, respectively, corresponding to 27.51% and 74.23% increases in degradation efficiency.

Moreover, XPS analysis results under varying ball-to-powder ratios was summarized in Fig. 7 and S1. Surface  $\text{Cu}^+$  increased from 21.6% to 31.8%, while bulk  $\text{Cu}^+$  decreased from 51.6% to 39.1%. Surface  $\text{Fe}^{2+}$  and  $\text{Fe}^{3+}$  rose by 94.04% and 21.57%, with corresponding bulk content decreases of 39.21% and 37.31%. Surface  $\text{S}^{2-}$  increased from 11.4% to 17.7%, while bulk metal-S dropped from 61.3% to 50.1%, and sulfate rose from 45.93% to 49.29%. These results confirm that a higher ball-to-powder ratio enhances exposure of active  $\text{Cu}^+/\text{Fe}^{2+}/\text{Fe}^{3+}/\text{S}^{2-}$  species and increases catalytic active sites. Additionally, it facilitates the

release of  $\text{Fe}/\text{Cu}$  into solution, boosting homogeneous Fenton activity and degradation efficiency.

Based on the above analyses, both surface area and chemical state changes induced by milling significantly influence catalytic performance. The optimal ball milling conditions were determined as a ball-to-powder ratio of 3 : 1 and milling time of 24 h.

### 3.3. Influence of ball milling parameters on catalyst microstructure and catalytic performance

**3.3.1. Determination of catalytic reaction system.** To select an appropriate catalytic system, the degradation performance of tetracycline in different reaction systems was investigated. The degradation curves are shown in Fig. 8. Due to the limited oxidative potential of  $\text{H}_2\text{O}_2$  ( $E = 1.77 \text{ V/SHE}$ ),  $\text{H}_2\text{O}_2$  alone had almost no degradation effect on tetracycline (2%,  $k_{\text{app}} = 0.002 \text{ min}^{-1}$ ). Under the condition of catalyst alone, although the degradation rate reached about 50%, adsorption played a significant role in this process, and the catalyst itself contributed minimally to degradation. Based on the UV-vis absorption spectrum of the catalyst, its band gap was calculated to be 1.42 eV, indicating that it can absorb visible light and thus potentially enhance its catalytic activity. However, in the “catalyst/light” system, apart from adsorption, no significant degradation occurred (10%,  $k_{\text{app}} = 0.016 \text{ min}^{-1}$ ), likely due to the high recombination rate of photo-generated electron-hole pairs, which reduces photocatalytic activity and thus the degradation rate. When using a heterogeneous Fenton-like system (catalyst/ $\text{H}_2\text{O}_2$ ), *i.e.*, adding  $0.50 \text{ g L}^{-1}$  of catalyst and  $3 \text{ mM H}_2\text{O}_2$  to the tetracycline solution, over 90% degradation was achieved within 10 minutes, with a reaction rate constant of

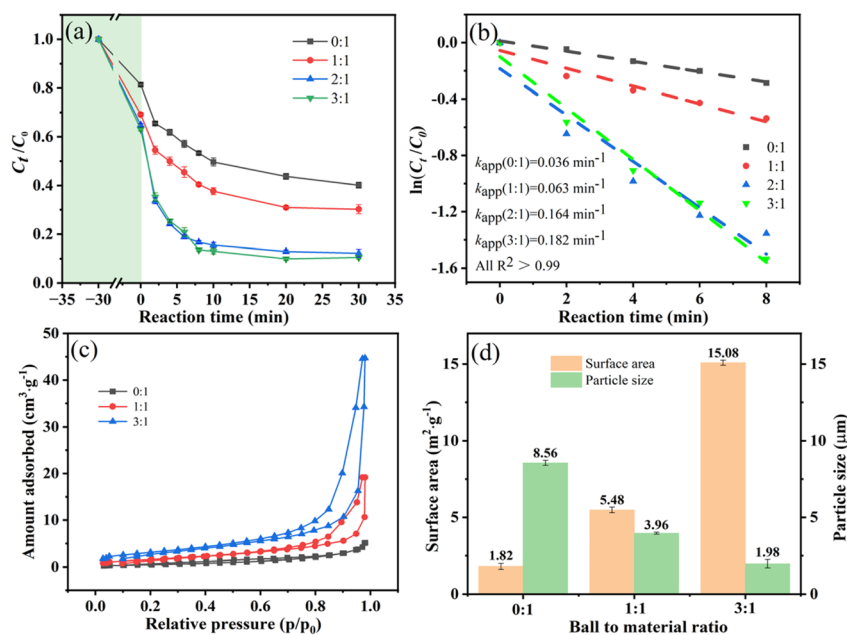


Fig. 6 (a) Tetracycline degradation curve, (b) catalytic reaction kinetics curve, (c) catalyst  $\text{N}_2$  adsorption-desorption curve, (d) catalyst specific surface area and average particle size. (Milling time: 24 h. Catalytic conditions: tetracycline concentration of  $20 \text{ mg L}^{-1}$ , catalyst dosage of  $0.50 \text{ g L}^{-1}$ ,  $\text{H}_2\text{O}_2$  dosage of  $3 \text{ mM}$ , initial pH value of 6.17; error bars represent standard deviation ( $n = 3$ )).



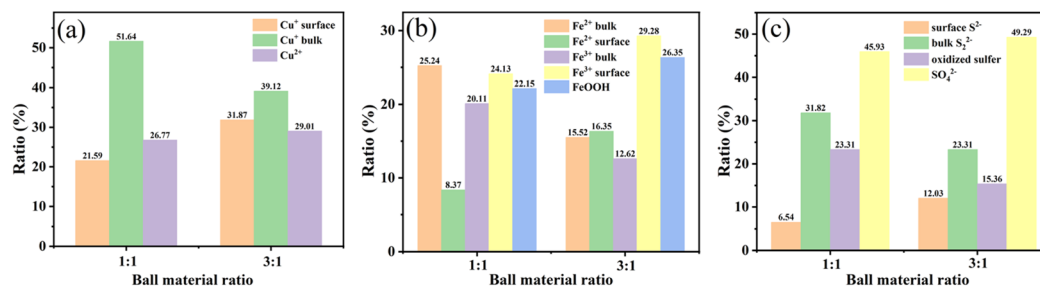


Fig. 7 Proportion of catalyst elements with different morphologies under different ball to material ratios: (a) Cu, (b) Fe, and (c) S.

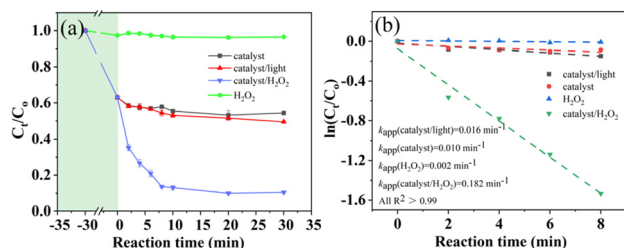


Fig. 8 (a) Degradation curves of tetracycline solutions in different reaction systems, (b) quasi first order kinetic curves. (Catalytic conditions: tetracycline concentration of 20 mg L<sup>-1</sup>, catalyst dosage of 0.50 g L<sup>-1</sup>, H<sub>2</sub>O<sub>2</sub> dosage of 3 mM, initial pH value of 6.17, simulated light intensity of 180 mW cm<sup>-2</sup> and the detailed parameters in Section S3; Error bars represent standard deviation ( $n = 3$ )).

0.182 min<sup>-1</sup>. The high efficiency of the “catalyst/H<sub>2</sub>O<sub>2</sub>” system may be attributed to the significant contents of Fe<sup>2+</sup> (16.35%) and Cu<sup>+</sup> (31.87%) on the surface of FeS<sub>2</sub>/CuFeS<sub>2</sub>, as revealed by XRD and XPS analyses. Both ions can react with surface-adsorbed H<sub>2</sub>O<sub>2</sub> to generate highly reactive hydroxyl radicals (<sup>•</sup>OH), leading to rapid and efficient degradation of tetracycline. Based on these results, the “catalyst/H<sub>2</sub>O<sub>2</sub>” system was selected for subsequent experiments.

**3.3.2. Influence of reaction parameters on tetracycline degradation.** The effects of catalyst dosage, H<sub>2</sub>O<sub>2</sub> concentration, and pH on tetracycline degradation in the “catalyst/H<sub>2</sub>O<sub>2</sub>” system were thoroughly investigated. Fig. 9a illustrates the effect of H<sub>2</sub>O<sub>2</sub> concentration, as H<sub>2</sub>O<sub>2</sub> increased from 1 mM to 3 mM, degradation efficiency rose from 72.12% to 90.11%

within 10 min. This is due to the more active radicals formed *via* interaction between H<sub>2</sub>O<sub>2</sub> and the catalyst. However, further increase to 5 mM yielded no significant improvement, possibly due to excess H<sub>2</sub>O<sub>2</sub> quenching <sup>•</sup>OH radicals (OH + OH → H<sub>2</sub>O<sub>2</sub>), thus reducing degradation efficiency.<sup>32–34</sup>

As shown in Fig. 9b, increasing the catalyst dosage from 0.25 g L<sup>-1</sup> to 0.5 g L<sup>-1</sup> increased the degradation rate from 82.23% to 90.11% in 10 minutes, likely due to more active sites and thus more <sup>•</sup>OH generation. However, increasing the dosage to 0.75 g L<sup>-1</sup> reduced efficiency to 81.32%, possibly due to excessive <sup>•</sup>OH scavenging and light scattering, which impaired catalytic performance.<sup>35,36</sup> Fig. 9c displays the effect of pH value. At pH 4–8, degradation reached about 90% in 10 min, with the optimal performance at pH 6.17, achieving 90.11%. At pH 11.86, efficiency dropped to 50.46%, indicating that high pH impedes degradation due to lower <sup>•</sup>OH oxidation potential and H<sub>2</sub>O<sub>2</sub> decomposition. Thus, the optimal conditions were: catalyst dosage of 0.5 g L<sup>-1</sup>, H<sub>2</sub>O<sub>2</sub> concentration of 3 mM, and pH 6.17 (initial pH value). Under these, 20 mg L<sup>-1</sup> tetracycline solution was degraded 90.11% within 10 min.

Based on the above analysis, the optimal conditions were determined as follows: catalyst dosage of 0.5 g L<sup>-1</sup>, H<sub>2</sub>O<sub>2</sub> concentration of 3 mM, and an initial pH of 6.17. Under these conditions, 90.11% of a 20 mg L<sup>-1</sup> tetracycline solution was degraded within 10 min. As shown in Table S1, the mechanically activated natural copper sulfide ore exhibits degradation efficiency comparable to or even higher than that of synthetic catalysts, but within a substantially shorter reaction time (10 min vs. 30–120 min).

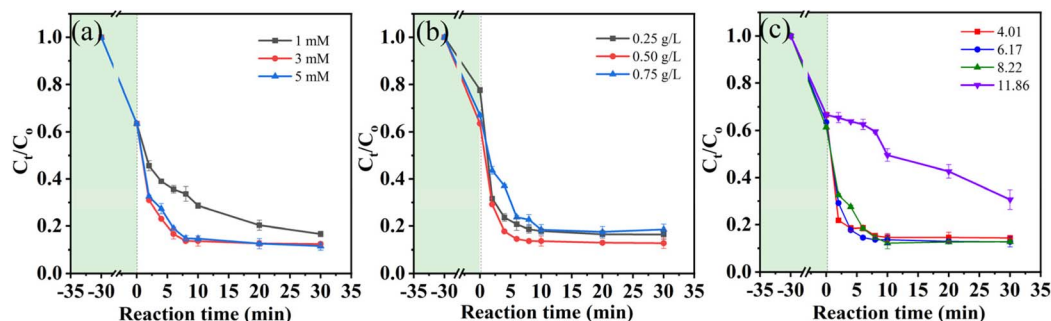


Fig. 9 Effects of different catalytic test parameters on tetracycline degradation: (a) H<sub>2</sub>O<sub>2</sub> content, (b) catalyst dosage, (c) pH value. (Error bars represent standard deviation ( $n = 3$ )).



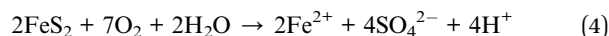
**3.3.3. Practical applicability in simulated wastewater.** The practical applicability of the mechanically activated copper sulfide ore catalyst was evaluated in simulated wastewater containing common inorganic ions ( $\text{Na}^+$ ,  $\text{NH}_4^+$ ,  $\text{Cl}^-$ ,  $\text{SO}_4^{2-}$ , each at 5 mM) and natural organic matter (humic acid, 20 mg L<sup>-1</sup>). As shown in Fig. S2, the catalyst maintained over 80% degradation efficiency within 30 min, demonstrating strong resistance to typical water matrix constituents. Its catalytic performance was further assessed for the degradation of metronidazole and ciprofloxacin under optimal conditions, achieving removal efficiencies of 88.35% and 74.71%, respectively, within 30 min (Fig. S3). These findings underscore the catalyst's potential for the effective removal of diverse organic pollutants in complex water environments.

### 3.4. Catalytic mechanism

**3.4.1. Identification of reactive species.** To elucidate the catalytic mechanism of copper sulfide ore, radical scavenging experiments were first conducted to identify the dominant reactive species. Fig. 10a gives the effect of various scavengers (Isopropanol (IPA), TEMPOL, and *L*-histidine) on tetracycline degradation. These agents selectively quench  $\cdot\text{OH}$ ,  $\cdot\text{O}_2^-$ , and  $^1\text{O}_2$ , respectively.<sup>2</sup> When 1 mM of each scavenger was added, the degradation rate significantly decreased from 90.11% to 48.56%, 60.17%, and 83.07%, respectively. The results indicate that  $\cdot\text{OH}$  is the main active species, followed by  $\cdot\text{O}_2^-$  and  $^1\text{O}_2$ . This was further confirmed *via* ESR spectroscopy (Fig. 10b), which revealed the characteristic peaks of  $\cdot\text{OH}$ ,  $\cdot\text{O}_2^-$ , and  $^1\text{O}_2$ . The strongest signal corresponded to  $\cdot\text{OH}$ , reaffirming its dominant role. To quantify the  $\cdot\text{OH}$  generation, terephthalic acid was used as a probe, and the  $\cdot\text{OH}$  concentration was monitored by fluorescence spectrophotometry (Fig. 10c). As the reaction progressed,  $\cdot\text{OH}$  levels steadily increased, reaching to 25  $\mu\text{M}$  after 10 min, indicating equilibrium. Beyond 20 min, the increase was marginal ( $\sim 27 \mu\text{M}$ ), and the degradation rate plateaued.

**3.4.2. Hybrid homogeneous-heterogeneous reaction nature.** Copper sulfide ore inevitably undergoes partial dissolution (eqn (4) and (5)), releasing Fe and Cu ions into solution, which can catalyze homogeneous Fenton reactions and impact tetracycline degradation. Under optimal conditions, the

concentrations of Fe and Cu ions were 5.78 mg L<sup>-1</sup> and 27.33 mg L<sup>-1</sup>, corresponding to dissolution rates of 3.54% and 25.33%, respectively. This suggests both homogeneous (dissolved ions) and heterogeneous (solid surface Fe/Cu) reactions contribute to the overall degradation.



To assess the contribution from the homogeneous pathway, 0.1 g of catalyst was stirred in 200 mL deionized water for 1 h, filtered through 0.45  $\mu\text{m}$  membranes, and then the filtrate was used for degradation experiments with 20 mg L<sup>-1</sup> tetracycline and 3 mM H<sub>2</sub>O<sub>2</sub>. As shown in Fig. 11, 59.83% degradation was achieved in 20 min, compared to 90.15% with the full catalyst. This suggests the homogeneous reaction contributes 66.36%, and the heterogeneous pathway contributes 33.64% to overall degradation. The hybrid homogeneous-heterogeneous nature offers several advantages over purely homogeneous Fenton systems. First, it reduces iron sludge generation, as the solid catalyst can be recovered and reused. Second, it allows operation over a wider pH range (pH 4–8, Fig. 9c), whereas conventional Fenton processes are optimal only under highly acidic conditions (pH 2–4). Third, the solid-phase Cu/Fe/S sites

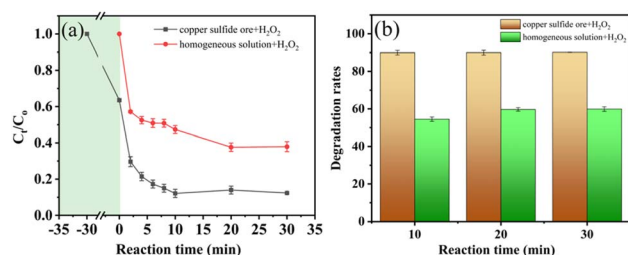


Fig. 11 (a) Degradation curves of tetracycline by copper sulfide ore and homogeneous solution, (b) the proportions of heterogeneous and homogeneous reactions under different degradation time (catalytic conditions: tetracycline concentration of 20 mg L<sup>-1</sup>, catalyst dosage of 0.50 g L<sup>-1</sup>, H<sub>2</sub>O<sub>2</sub> dosage of 3 mM; error bars represent standard deviation ( $n = 3$ )).

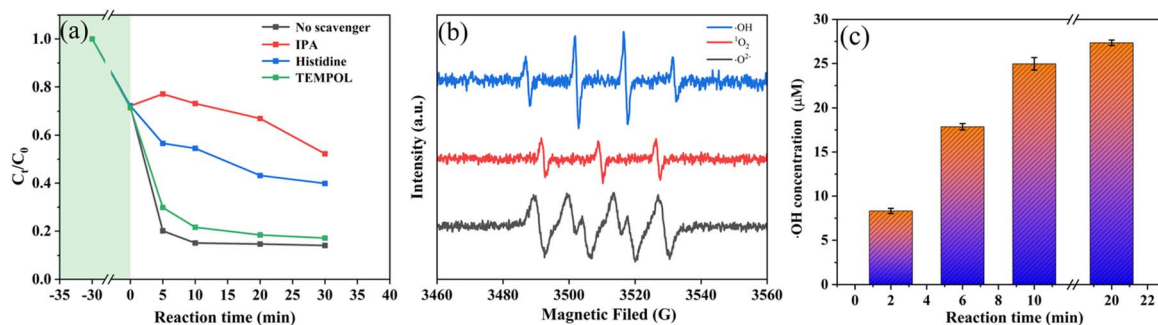


Fig. 10 (a) Effects of different scavengers on the degradation of tetracycline in the catalytic system (catalytic conditions: tetracycline concentration of 20 mg L<sup>-1</sup>, catalyst dosage of 0.50 g L<sup>-1</sup>, H<sub>2</sub>O<sub>2</sub> dosage of 3 mM, quencher concentration of 1 mM), (b) ESR spectra of DMPO- $\cdot\text{OH}$ , DMPO- $\cdot\text{O}_2^-$  and TMPO- $^1\text{O}_2$  adducts, (c) the generation of  $\cdot\text{OH}$  radicals varies over time.



provide continuous regeneration of reactive species *via* electron transfer from reduced sulfur species.

However, this hybrid mechanism also has implications for catalyst longevity. The dominance of the homogeneous pathway implies that sustained catalytic activity depends on continuous dissolution of metal ions from the solid surface. Over multiple cycles, this leads to gradual metal depletion and activity decline, as discussed in Section 3.5. Thus, while the hybrid system offers enhanced initial kinetics, long-term operation may require strategies such as periodic replenishment of metal ions or pH-controlled precipitation to recover leached species.

**3.4.3. Ion synergistic enhancement mechanism.** Based on the XRD pattern (Fig. 1), the quantitative analysis of copper sulfide concentrate was carried out using the JADE Pro software through the full-spectrum fitting - Rietveld method (Section S4). The results indicate that its main phase compositions were pyrite and chalcopyrite, and their mass percentages were 38 wt% and 62 wt% respectively (Fig. S4 and S5). In order to investigate the influence of different types of ions in the catalyst on the degradation of tetracycline and the interaction between different ions, degradation experiments were carried out using pyrite, chalcopyrite, and copper sulfide concentrate separately. The results were shown in Fig. 12

Results indicate that pyrite and chalcopyrite alone degraded tetracycline rapidly in the first 5 min (74.40% and 60.20%, respectively), reaching equilibrium around 81.80% and 82.80% after 30 min. Chalcopyrite showed slightly lower activity. In contrast, the combined copper sulfide ore achieved about 90% degradation within 10 min with faster kinetics, suggesting synergistic interactions between Fe and Cu ions.  $\text{Fe}^{2+}$  released into solution dominates the activation of  $\text{H}_2\text{O}_2$  to produce  $\cdot\text{OH}$ ,  $\cdot\text{O}_2^-$ , and  $^1\text{O}_2$  (eqn (6)–(10)), homogeneous Fenton reactions). The  $\equiv\text{Fe}^{2+}/\text{Fe}^{3+}$  and  $\equiv\text{Cu}^+$  ions on the solid surface promote the heterogeneous catalytic reaction of  $\text{H}_2\text{O}_2$  to generate reactive oxygen species ( $(E^\theta(\text{H}_2\text{O}_2/\text{H}_2\text{O}) = 1.776 \text{ V}$ ,  $E^\theta(\text{Fe}^{3+}/\text{Fe}^{2+}) = 0.770 \text{ V}$ ,  $E^\theta(\text{Cu}^{2+}/\text{Cu}^+) = 0.166 \text{ V}$  (eqn (11)–(14)), heterogeneous Fenton reactions)).

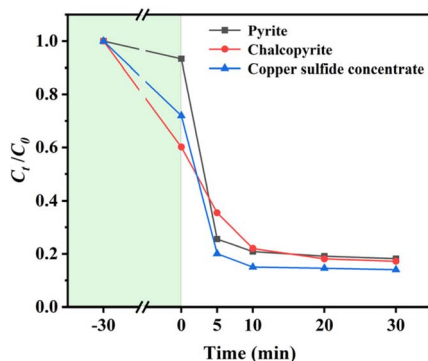
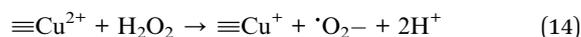
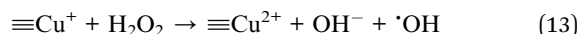
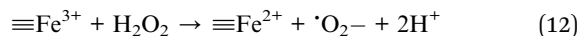
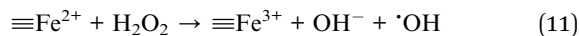
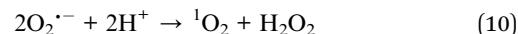
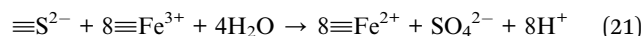
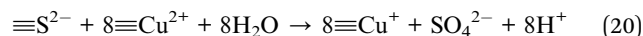
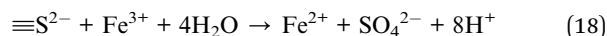
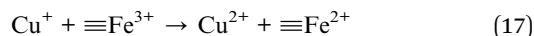
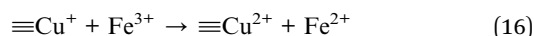


Fig. 12 Degradation curves of tetracycline solution in pyrite, chalcopyrite and copper sulfide concentrate (copper sulfide concentrate dosage of  $0.50 \text{ g L}^{-1}$ , pyrite dosage of  $0.19 \text{ g L}^{-1}$ , chalcopyrite dosage of  $0.31 \text{ g L}^{-1}$ ,  $\text{H}_2\text{O}_2$  concentration of  $3 \text{ mM}$ , pH value of the initial pH, tetracycline concentration of  $20 \text{ mg L}^{-1}$ ).



Meanwhile, based on the comparison of electrode potentials between Fe and Cu ions, redox cycles between  $\text{Fe}^{3+}/\text{Fe}^{2+}$  and  $\text{Cu}^{2+}/\text{Cu}^+$  (eqn (15)–(17)) facilitate electron transfer and boost degradation efficiency. In addition, the reducing sulfur ( $\text{S}^{2-}$ ,  $\text{S}_2^{2-}$ ) in the catalyst can act as an electron mediator ( $(E^\theta(\text{SO}_4^{2-}/\text{S}^{2-}) = 0.146 \text{ V})$ , promoting the reduction of  $\text{Fe}^{3+}$  to  $\text{Fe}^{2+}$  and  $\text{Cu}^{2+}$  to  $\text{Cu}^+$  and accelerating the ionic redox cycle (eqn (18)–(21)), thus further accelerating the degradation reaction.



The redox cycling between  $\equiv\text{Fe}^{3+}/\equiv\text{Fe}^{2+}$  and  $\equiv\text{Cu}^{2+}/\equiv\text{Cu}^+$  is experimentally supported by XPS analysis before and after reaction (Fig. 13 and S6), which shows a decrease in  $\equiv\text{Fe}^{2+}$  (from 19.24% to 9.85%) and  $\equiv\text{Cu}^+$  (from 66.42% to 60.71%), consistent with their participation in electron transfer reactions. Additionally, the involvement of reduced sulfur species ( $\text{S}^{2-}$ ,  $\text{S}_2^{2-}$ ) as electron mediators is inferred from the two evidence. First, XPS shows a decrease in reductive  $\text{S}_2^{2-}$  (from 44.42% to 30.49%) and a corresponding increase in oxidized  $\text{SO}_4^{2-}$  (from 34.53% to 49.23%) after reaction. Second, the standard electrode potential of  $\text{SO}_4^{2-}/\text{S}^{2-}$  (0.146 V) is thermodynamically favorable for mediating electron transfer between  $\text{Fe}^{3+}/\text{Fe}^{2+}$  and  $\text{Cu}^{2+}/\text{Cu}^+$ . Direct experimental verification would require advanced techniques which are planned for future work.

Based on this, a degradation mechanism (Fig. 14) is proposed. And the “copper sulfide ore- $\text{H}_2\text{O}_2$ ” system degrades



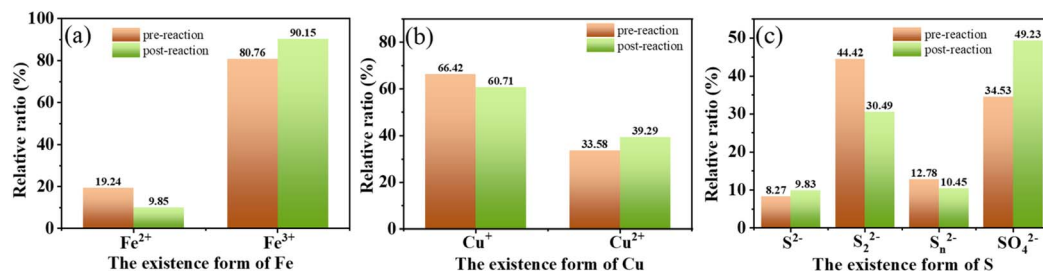


Fig. 13 Relative contents of different elements in the catalyst before and after the reaction: (a) Fe, (b) Cu, (c) S.

tetracycline *via* synergistic homogeneous (66.36%) and heterogeneous (33.64%) Fenton-like reactions. Among them, homogeneous catalysis significantly improves the degradation rate and degradation speed of tetracycline. Under the optimized experimental conditions, more than 90% of tetracycline can be degraded within 5 min. Meanwhile, the redox cycles of  $\equiv\text{Fe}^{3+}/\text{Fe}^{2+}$  and  $\equiv\text{Cu}^{2+}/\text{Cu}^{+}$  in the system, supplemented by the electron transfer effect of reducing sulfur in the catalyst, jointly accelerate the ion cycle and further drive efficient degradation.

However, the progressive oxidation of reduced sulfur species to sulfate affects the long-term catalytic performance. Over multiple reaction cycles, the gradual depletion of  $\text{S}^{2-}$  and  $\text{S}_2^{2-}$  (Fig. 13c) reduces the availability of electron mediators, potentially hindering the  $\text{Fe}^{3+}/\text{Fe}^{2+}$  and  $\text{Cu}^{2+}/\text{Cu}^{+}$  redox cycles. This likely contributes to the decline in activity observed over five cycles (Section 3.5), in addition to metal leaching.

### 3.5. Reusability and stability

The reusability of a heterogeneous Fenton-like catalyst is essential for its practical viability in wastewater treatment. Five consecutive degradation cycles were performed under optimal reaction conditions (catalyst dosage  $0.5 \text{ g L}^{-1}$ ,  $\text{H}_2\text{O}_2$   $3 \text{ mM}$ , initial TC concentration  $20 \text{ mg L}^{-1}$ ,  $\text{pH} \approx 6.10$ ), with the catalyst being recovered, washed with ethanol, and dried before each reuse. As shown in Fig. 15a, the tetracycline degradation efficiency remained above 65% after five cycles, demonstrating satisfactory recyclability. Correspondingly, the TOC removal

efficiency decreased from 43.58% to 31.69% over the cycles (Fig. 15b), suggesting that while the overall oxidation rate slows, the catalyst retains its ability to mineralize intermediates once they are formed. This is consistent with the heterogeneous sites remaining active even as the homogeneous contribution diminishes.

The slight decline in catalytic performance across cycles is primarily attributed to the progressive leaching of copper species from the mineral surface. ICP-OES analysis revealed cumulative  $\text{Cu}^{2+}$  leaching of about  $27.327 \text{ mg L}^{-1}$  after the fifth cycle (Tables S6 and S7), which exceeds the permissible discharge limit for industrial wastewater in many jurisdictions (typically  $<2.0 \text{ mg L}^{-1}$ ). This represents a trade-off, namely, the same leaching that enhances homogeneous catalytic activity also poses environmental concerns and limits catalyst longevity. However, this issue can be effectively mitigated through a simple post-treatment step. Adjusting the effluent pH to 10.40–11.16 with  $\text{Ca}(\text{OH})_2$  induces precipitation of copper hydroxide, reducing dissolved  $\text{Cu}^{2+}$  to below  $0.35 \text{ mg L}^{-1}$ , well within typical discharge standards. The precipitated copper could potentially be recovered and recycled.

Furthermore, the decline in activity (from 90.1% to 65.3% over five cycles) correlates with cumulative Cu loss, suggesting that leaching, rather than surface deactivation, is the primary cause of performance degradation. Under continuous operation, the catalyst would likely require periodic replenishment or regeneration after 3–5 cycles to maintain  $>80\%$  efficiency.

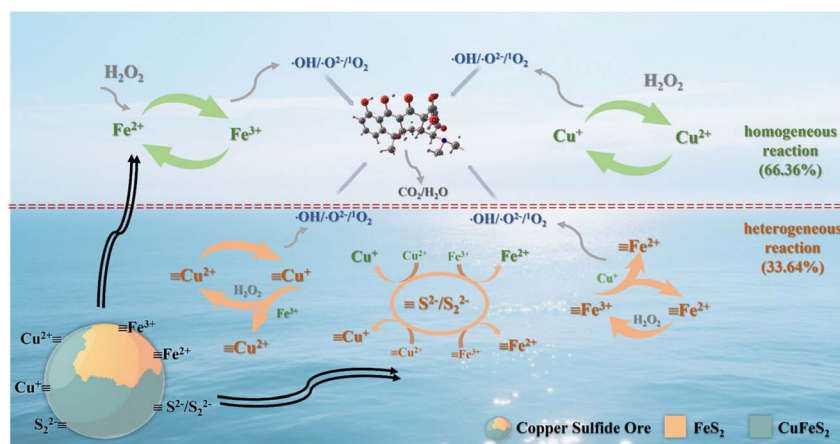


Fig. 14 Schematic diagram of catalytic degradation mechanism.



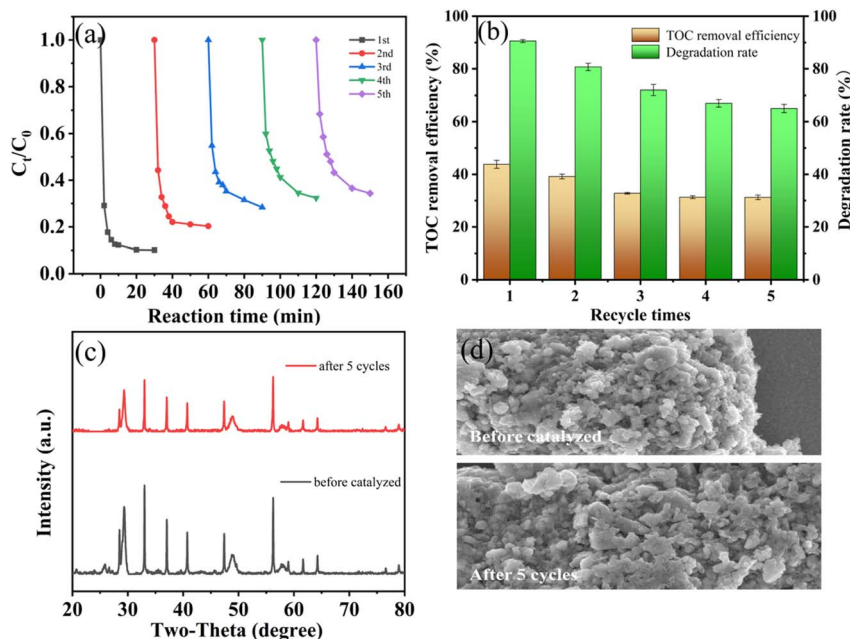


Fig. 15 (a and b) Tetracycline degradation efficiency and TOC removal rate after five cycles, (c and d) XRD and SEM images before and after catalyst reaction.

Despite the gradual metal leaching, structural characterization revealed excellent physicochemical stability of the catalyst. XRD patterns (Fig. 15c) showed no significant phase transformation after cycling, with characteristic peaks of  $\text{FeS}_2$  and  $\text{CuFeS}_2$  remaining clearly identifiable. SEM images (Fig. 15d) further confirmed that the catalyst maintained its original morphology and particle size distribution without obvious aggregation or disintegration. These findings collectively indicate that natural copper sulfide ore exhibits not only strong catalytic activity and reusability but also the structural robustness necessary for repeated applications in antibiotic wastewater treatment. Moreover, metal leaching can be effectively managed *via* straightforward pH-controlled precipitation. For practical implementation, a two-stage process is proposed: (i) catalytic degradation in a stirred tank reactor, followed by (ii) a settling tank where effluent pH is adjusted to precipitate dissolved metals. This design ensures that treated water meets

discharge standards while enabling recovery and reuse of the solid catalyst.

### 3.6. Degradation pathway analysis

To elucidate the degradation pathways, HPLC-MS was used to identify the byproducts (Table S8 and Fig. 16). Major intermediates showed reduced antimicrobial activity in preliminary bioassay tests. Based on  $m/z$  values, two primary pathways were proposed.

Pathway ①: Tetracycline ( $m/z = 445$ ) undergoes ring cleavage and methyl migration to form an intermediate ( $m/z = 397$ ), which then experiences carbon chain scission with hydroxylation or decarboxylation, forming products  $m/z = 284$  and  $m/z = 298$ , which were characterized by ring-opening and functional group rearrangement.

Pathway ②: Tetracycline first undergoes demethylation to  $m/z = 434$ , followed by dehydration to  $m/z = 416$ . Further hydroxylation and ring cleavage yield  $m/z = 370$ , eventually forming short-chain polyhydroxy intermediates ( $m/z = 276$ ), with reduced carbon chain length and increased hydroxyl groups.

Both pathways ultimately mineralize tetracycline into small inorganic molecules such as  $\text{H}_2\text{O}$ ,  $\text{CO}_2$ , and  $\text{NO}_3^-$  *via* deep oxidation and ring opening.

## 4. Conclusion

This study investigated mechanically activated copper sulfide ore for Fenton-like catalytic degradation of tetracycline, yielding the following conclusions. Mechanical activation significantly enhances the catalytic performance of copper sulfide concentrate. Optimal ball-milling conditions were found to be a ball-to-

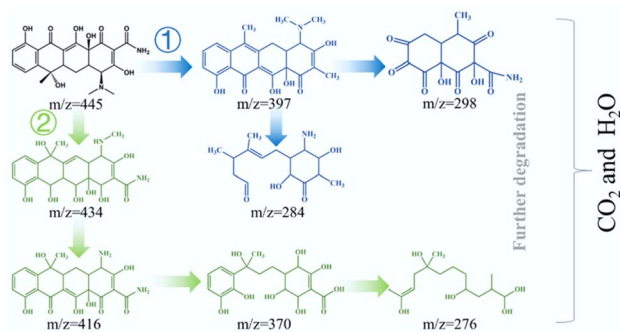


Fig. 16 Schematic diagram of tetracycline degradation pathway.



powder ratio of 3 : 1 and milling time of 24 hours. Under these conditions, the “copper sulfide–H<sub>2</sub>O<sub>2</sub>” system achieved 90.11% tetracycline degradation within 10 min and TOC removal up to 43.58%. This improvement is due to the refined particle size and increased surface area, exposing more Cu/Fe/S sites and enhancing catalytic activity. The degradation mechanism involves both homogeneous (66.36%) and heterogeneous (33.64%) catalysis. Mechanical activation promotes ion release (Cu<sup>2+</sup>/Fe<sup>2+</sup>/SO<sub>4</sub><sup>2-</sup>), enhancing homogeneous reactions. In heterogeneous reactions, Fe and Cu ions accelerate redox cycles *via* electron transfer, further aided by reduced sulfur species (S<sup>2-</sup>, S<sub>2</sub><sup>2-</sup>) acting as electron mediators to regenerate Fe<sup>2+</sup> and Cu<sup>+</sup>, driving rapid degradation. Two degradation pathways were identified *via* HPLC-MS, both ending in deep oxidation and mineralization to H<sub>2</sub>O, CO<sub>2</sub>, and NO<sub>3</sub><sup>-</sup>. This work establishes a high-efficiency heterogeneous Fenton-like system based on naturally occurring polymetallic sulfide ores, demonstrating great potential for antibiotic wastewater treatment.

## Author contributions

Lizheng Gou: writing: original draft, visualization, investigation. Xiwang Miao: writing: review & editing, formal analysis. Yuhang Liu: investigation, formal analysis. Mei Zhang: supervision, project administration. Min Guo: writing – review & editing, supervision, project administration, funding acquisition.

## Conflicts of interest

The author reported no potential conflicts of interest

## Data availability

The data supporting this article have been included as part of the supplementary information (SI). Supplementary information is available. See DOI: <https://doi.org/10.1039/d5ra09931e>.

## Acknowledgements

This work was supported by the National Natural Science Foundation of China (No. 52572312, U24A20555).

## Notes and references

- C. Li, M. K. Awasthi, J. Liu and T. Yao, *Environ. Res.*, 2025, **266**, 120417.
- S. Qiu, L. Gou, F. Cheng, M. Zhang and M. Guo, *J. Environ. Manage.*, 2022, **302**, 114119.
- J. Liu, Y. Hu, X. Li, Y. Liu, Y. Chen, J. Cheng, X. Zhu, G. Wang and J. Xie, *Chem. Eng. J.*, 2025, **511**, 162009.
- L. Jian, X. Sun, P. Zhao, X. Meng and Y. Dong, *Chem. Eng. J.*, 2025, **515**, 163871.
- M. Han, H. Wang, W. Jin, W. Chu and Z. Xu, *J. Environ. Sci.*, 2023, **128**, 181–202.
- Y. Lin, J. Qiao, Y. Sun and H. Dong, *J. Environ. Sci.*, 2025, **147**, 114–130.
- X. Huang, T. Zhu, W. Duan, S. Liang, G. Li and W. Xiao, *J. Hazard. Mater.*, 2020, **381**, 120998.
- Y. Vieira, M. B. Ceretta, E. L. Foletto, E. A. Wolski and S. Silvestri, *J. Water Proc. Eng.*, 2020, **36**, 101397.
- A. Cheng, Y. He, X. Liu and C. He, *J. Environ. Sci.*, 2024, **136**, 390–399.
- J. Jiang, J. Gao, S. Niu, X. Wang, T. Li, S. Liu, Y. Lin, T. Xie and S. Dong, *J. Environ. Sci.*, 2021, **106**, 147–160.
- D. Rickard and G. W. Luther, *Chem. Rev.*, 2007, **107**, 514–562.
- P. Engesgaard and K. L. Kipp, *Water Resour. Res.*, 1992, **28**, 2829–2843.
- X. Chen, Y. Han, P. Gao and H. Li, *Sep. Purif. Technol.*, 2021, **274**, 118817.
- X. Lin, J. Hu, Z. Mo, Z. Wang, R. Wang and J. Liang, *J. Environ. Manage.*, 2024, **365**, 121607.
- W. Liu, Y. Wang, Z. Ai and L. Zhang, *ACS Appl. Mater. Interfaces*, 2015, **7**, 28534–28544.
- R. Matta, K. Hanna and S. Chiron, *Sci. Total Environ.*, 2007, **385**, 242–251.
- H. Che, S. Bae and W. Lee, *J. Hazard. Mater.*, 2011, **185**, 1355–1361.
- J. Da Silveira Salla, G. L. Dotto, D. Hotza, R. Landers, K. Da Boit Martinello and E. L. Foletto, *J. Environ. Chem. Eng.*, 2020, **8**, 104077.
- X. Xu, D. Tang, J. Cai, B. Xi, Y. Zhang, L. Pi and X. Mao, *Appl. Catal. B Environ.*, 2019, **251**, 273–282.
- J. Yang, R. Huang, Y. Cao, H. Wang, A. Ivanets and C. Wang, *Environ. Sci. Pollut. Res.*, 2022, **29**, 75651–75663.
- W. Nie, Q. Mao, Y. Ding, Y. Hu and H. Tang, *J. Hazard. Mater.*, 2019, **364**, 59–68.
- J. Wang, J. Yao, Y. Li, Z. Wei, C. Gao, L. Jiang and X. Wu, *J. Hazard. Mater.*, 2024, **467**, 133751.
- C. Li, L. Zhu, C. Yan, J. Yao, J. Zhu, D. Ji and B. Wang, *Environ. Res.*, 2025, **284**, 122263.
- C. Fang, R. Li, Y. Zheng and L. Nie, *Dalton Trans.*, 2025, **54**, 9605–9614.
- C. Boekema, A. M. Krupski, M. Varasteh, K. Parvin, F. Van Til, F. Van Der Woude and G. A. Sawatzky, *J. Magn. Magn. Mater.*, 2004, **272–276**, 559–561.
- J. Da Silveira Salla, K. Da Boit Martinello, G. L. Dotto, E. García-Díaz, H. Javed, P. J. J. Alvarez and E. L. Foletto, *Colloids Surf., A Physicochem. Eng. Asp.*, 2020, **595**, 124679.
- A. Ghahremaninezhad, D. G. Dixon and E. Asselin, *Electrochim. Acta*, 2013, **87**, 97–112.
- S. Xin, G. Liu, X. Ma, J. Gong, B. Ma, Q. Yan, Q. Chen, D. Ma, G. Zhang, M. Gao and Y. Xin, *Appl. Catal. B Environ.*, 2021, **280**, 119386.
- S. Xu, M. Zanin, W. Skinner and S. Brito E Abreu, *Miner. Eng.*, 2021, **170**, 106992.
- J. Yao, J. Liu, Z. Wei, Y. Li, H. Zhou, J. Wang, W. Li, Q. Zhang and X. Wu, *Mater. Res. Bull.*, 2023, **164**, 112275.
- Z. Zhao, Z. Zhou, X. Zhang, C. Hou and D. Wu, *Sci. Total Environ.*, 2024, **952**, 175833.
- X. Han, L. Gou, S. Tang, F. Cheng, M. Zhang and M. Guo, *J. Environ. Manage.*, 2021, **283**, 111941.



- 33 Z. Wang, C. Lai, L. Qin, Y. Fu, J. He, D. Huang, B. Li, M. Zhang, S. Liu, L. Li, W. Zhang, H. Yi, X. Liu and X. Zhou, *Chem. Eng. J.*, 2020, **392**, 124851.
- 34 J. Zhou, F. Ma, H. Guo and D. Su, *Appl. Catal. B Environ.*, 2020, **269**, 118784.
- 35 Y. Li, J. He, K. Zhang, P. Hong, C. Wang, L. Kong and J. Liu, *J. Mater. Sci.*, 2020, **55**, 13767–13784.
- 36 X. Zhang, B. Ren, X. Li, B. Liu, S. Wang, P. Yu, Y. Xu and G. Jiang, *J. Hazard. Mater.*, 2021, **418**, 126333.

